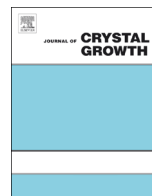




ELSEVIER

Contents lists available at ScienceDirect

Journal of Crystal Growth

journal homepage: www.elsevier.com/locate/jcrysgr

Low temperature AlN growth by MBE and its application in HEMTs



Faiza Afroz Faria*, Kazuki Nomoto, Zongyang Hu, Sergei Rouvimov, Huili (Grace) Xing, Debdeep Jena

Department of Electrical Engineering, University of Notre Dame, Notre Dame, IN 46556, USA

ARTICLE INFO

Article history:

Received 31 October 2014

Accepted 22 March 2015

Communicated by Dr. A. Brown

Available online 29 April 2015

Keywords:

A1. AlN

A1. Atomic force microscopy

A1. X-ray diffraction

A1. Transmission electron microscopy

A3. Molecular beam epitaxy

B3. High electron mobility transistor

ABSTRACT

Low temperature growth of AlN from 470 °C down to room temperature has been studied by RF-plasma assisted molecular beam epitaxy (PAMBE). Partially amorphous AlN was achieved at growth temperatures below 250 °C. We demonstrate the application of the low temperature (LT-) AlN as an in-situ surface passivation technique for III-nitride based high electron mobility transistors (HEMTs). High 2DEG densities $> 2 \times 10^{13} \text{ cm}^{-2}$ and sheet resistance $< 250 \Omega/\square$ at room temperature were first obtained for MBE grown AlN/GaN HEMT structures with thin high temperature AlN barrier, then capped with LT-AlN ($< 4 \text{ nm}$). Using this novel technique, low DC-RF dispersion with gate lag and drain lag below 2% is demonstrated for an AlN/GaN HEMT.

© 2015 Elsevier B.V. All rights reserved.

1. Introduction

MBE growth of AlN at low temperature ($< 600 \text{ °C}$) has not been explored and a systemic study of it is still missing. Epitaxial growth of high quality single crystal AlN is possible at high temperatures, preferably above 700 °C using metal-organic chemical vapor deposition (MOCVD) or MBE. This is due to the fact that Al has low adatom mobility at low growth temperatures. In contrast, low temperature growth of AlN is common in other thin film deposition techniques, such as, atomic layer deposition (ALD), plasma enhanced chemical vapor deposition (PECVD) or sputter deposition. The quality of the AlN films obtained by these techniques differs from the MBE or MOCVD grown AlN in terms of crystallinity. MBE and MOCVD are employed to achieve single crystal AlN. On the other hand, ALD, PECVD or sputtering techniques are used for applications in which single crystal AlN is not essential.

In this work, we perform a systematic study of low temperature MBE growth of AlN. We investigate the possible application of MBE grown LT-AlN as an in-situ surface passivation layer for performance enhancement of III-nitride HEMTs. Although reports of various passivation techniques exist in literature [1–6], further improvement is desired. DC-RF dispersion in HEMTs is an issue still to be addressed effectively by the III-nitride community [7]. AlN has a wide bandgap ($\sim 6.2 \text{ eV}$) and a high thermal conductivity (285 W/m/K for wurtzite single crystal) [8]. Its unique properties make it a strong candidate compared to other materials typically

chosen for III-nitride surface passivation [1–4]. Furthermore, in-situ passivation within the ultra high vacuum environment of MBE prevents the surface from being exposed to atmosphere/moisture before it is passivated. Therefore, MBE offers an advantage over other tools used for ex-situ passivation, for example, ALD or PECVD. To the best of our knowledge, the MBE grown LT-AlN, and its application for in-situ passivation of III-nitride surfaces have not been reported yet. The aim of this work is to provide some insight into this rather unexplored field of III-nitride research.

2. MBE growth of low temperature AlN

All III-nitride growths in this work were performed using a Veeco Gen 930 RF-plasma assisted MBE system. The growths were done along the [0 0 0 1] direction on *c*-plane substrates. Reflection high-energy electron diffraction (RHEED) was used for in-situ film characterization. For ex-situ structural characterization of the MBE grown films, Atomic Force microscopy (AFM), X-ray diffraction (XRD) and Transmission electron microscopy (TEM) were used.

2.1. AlN films grown at different temperatures

The goal of the first experiment was to study the change in structural properties of AlN as a function of the growth temperature. A series of AlN/GaN (15/50 nm) films were grown on semi-insulating (SI) GaN on Sapphire templates prepared by MOCVD. The growth of 50 nm GaN was performed under slightly metal-rich conditions at $T_{\text{TC}} \sim 660 \text{ °C}$ as measured by the thermocouple.

* Corresponding author.

E-mail addresses: ffaria@nd.edu, faizafaria2011@yahoo.com (F.A. Faria).

The excess Ga was desorbed in-situ at $T_{Tc} \sim 700$ °C before growing the AlN layer. Five 15 nm thick AlN layers were grown at $T_{Tc} \sim 800$, 660, 470, 250 °C and at room temperature (RT) with Al/N flux ~ 1 . A growth interruption (GI) was applied to reach the desired temperature before growing the AlN layer. A growth rate of ~ 180 nm/h was used with a RF-plasma power of 190 W and a nitrogen flow rate of 1.1 sccm.

To characterize the films, ω - 2θ scan along the 002 reflection were performed using XRD. The presence of the AlN peaks in addition to the GaN substrate peaks are observed in all 5 samples (Fig. 1). However, the FWHM of the AlN peak increases with decreasing growth temperature. This is expected as the quality of the single crystal AlN degrades at lower growth temperature and the film becomes less oriented along the c -axis. Due to the $\sim 2.4\%$ lattice mismatch, AlN grown on GaN is tensile strained and beyond a critical thickness of ~ 6.5 nm it starts to crack [9]. In this experiment, the thickness of the AlN films grown on GaN was larger than the critical thickness. AFM images show cracks on the surface of the 15 nm AlN layers grown at $T_{Tc} \sim 800$, 660 and 470 °C (Fig. 2a–c, respectively). The density of the cracks reduces by more than 50% as T_{Tc} is lowered from 800 to 470 °C. No cracks are observed on the surface of the 15 nm AlN grown on GaN at $T_{Tc} \sim 250$ °C and at RT (Fig. 2d and e). A possible explanation of this observation would be the difference in thermally-induced stress in AlN when grown on GaN at different temperatures. Figge et al., experimentally calculated the thermal expansion coefficient of wurtzite AlN as a function of temperature [10]. Based on their hypothesis, the mismatch between the in-plane lattice constants of AlN and GaN induced only by thermal expansion is maximum

($\sim 0.055\%$) at a temperature of ~ 700 K (427 °C). As temperature is decreased beyond this value, the thermally-induced mismatch decreases monotonically. So, a low growth temperature as opposed to conventional high temperature (> 600 °C) may reduce the possibility of crack formation as the substrate is cooled down. The AFM image in Fig. 2d shows presence of pits on the AlN surface for $T_{Tc} \sim 250$ °C. However, no pits are observed and atomic steps do not appear on the surface of the AlN grown at RT (Fig. 2e) unlike high quality single crystal AlN. The RMS roughness of the AlN film is plotted as a function of growth temperature in Fig. 3.

2.2. AlN growth below 250 °C

To further study the crystal quality of AlN grown at low temperature ($T_{Tc} < 250$ °C), the following experiment was performed. A 15 nm thick AlN film was grown at RT under slightly N-rich regime on a GaN on sapphire template. The Al/N flux ratio was ~ 0.97 . Under similar growth condition, a thicker (~ 200 nm) AlN film was grown on a similar template. A control sample was prepared by growing 15 nm AlN at a high temperature of $T_{Tc} \sim 660$ °C on a similar substrate. In-situ measurement by RHEED showed 1×1 reconstruction for the GaN substrate and the high temperature (HT-) AlN oriented along the c -axis. On the other hand, diffused ring like features were observed in RHEED for the AlN films grown at RT. This indicates polycrystalline quality of the films near the surface. The ω - 2θ scan along the 002 reflection (Fig. 4) shows the AlN peak only for the control sample. The absence of AlN peak for the other two samples suggests that the RT AlN is not oriented along the $[0001]$ direction and is partially or fully amorphous [11].

AFM scans over large ($400 \mu\text{m}^2$) and small ($4 \mu\text{m}^2$) areas reveal that the surface roughness is relatively higher for the 200 nm thick film compared to the 15 nm film (Fig. 5). A relatively higher density of accumulated metal is observed on the surface of the thicker film (Fig. 5a and b). However, both 15 and 200 nm films show RMS roughness < 1 nm over small areas (Fig. 5c and d). The lack of adatom mobility of Al at room temperature leads to the formation of occasional voids and accumulation of Al on the surface. For thicker films this effect is more pronounced. Further studies by varying the Al/N flux ratio in N-rich regime and by applying shutter modulation method may lead to a better understanding of the surface roughness limits of PAMBE grown RT AlN.

To further analyze the structural property of LT-AlN grown on different substrates, the following experiment was performed. MOCVD grown AlN on sapphire and SI GaN on sapphire were chosen as the substrates. The substrates were co-loaded into the reactor chamber and ~ 130 nm LT-AlN films were grown. The targeted growth temperature was $T_{Tc} \sim 160$ °C. Al/N flux ratio was ~ 1 . The RF plasma power was set to 275 W with a nitrogen flow rate of 1.25 sccm to achieve a growth rate of ~ 260 nm/h. A ω - 2θ scan along the 002 reflection was performed for the 130 nm LT-AlN film grown

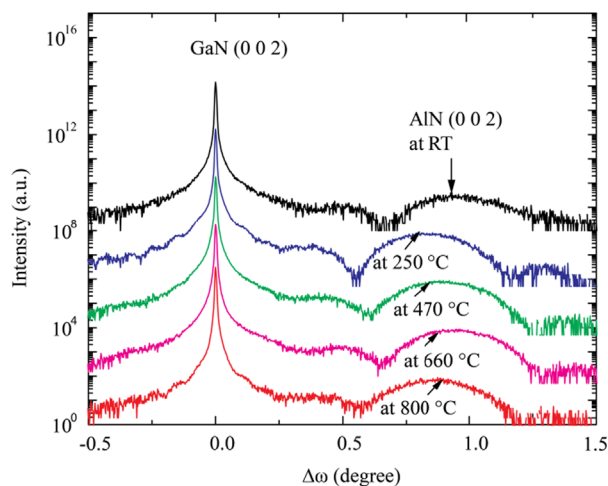


Fig. 1. ω - 2θ scan along the 002 reflection for the series of 5 samples show peak for 15 nm AlN grown at different temperatures on GaN.

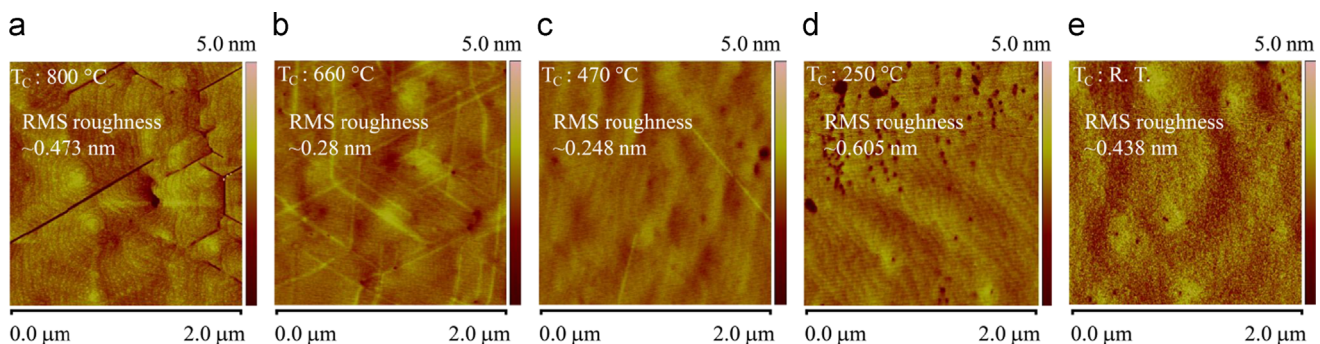


Fig. 2. AFM scan over an area of $4 \mu\text{m}^2$ shows the surface morphology of the 15 nm AlN grown at different temperatures on GaN.

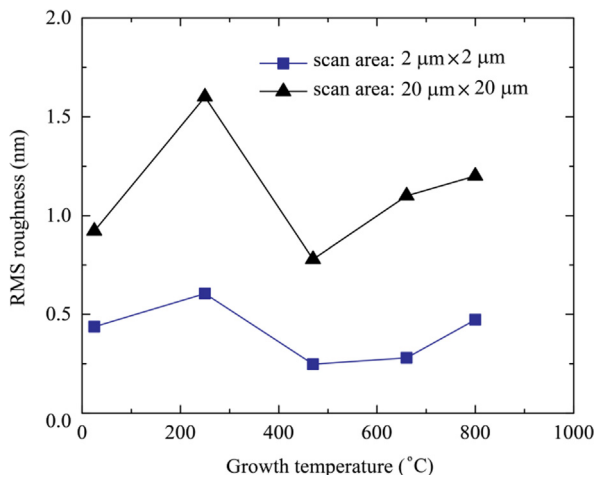


Fig. 3. RMS roughness obtained from AFM scan of the 15 nm AlN films grown at different temperatures on GaN.

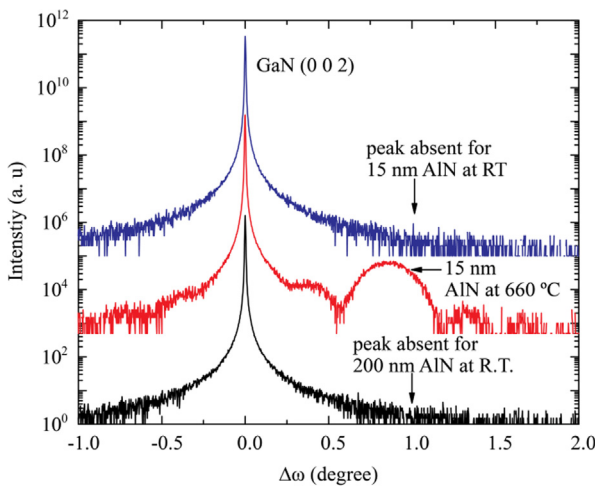


Fig. 4. ω - 2θ scan along the 002 reflection show the absence of AlN peak for 15 and 200 nm AlN grown at RT on GaN templates. The peak for the 15 nm AlN grown at 660 °C on a similar GaN template is present.

on Si GaN substrate. The AlN peak was absent. Cross-section TEM image confirms that continuous films of ~ 130 nm LT-AlN were grown on both substrates with no preferential orientation. The coexistence of polycrystalline and amorphous regions within the LT-AlN film is manifested in both samples (Fig. 6b and c). The inset of Fig. 6c shows the Fast Fourier Transform (FFT) for the region highlighted in the LT-AlN film. The FFT represents the diffraction pattern of that region and confirms the presence of amorphous region in the LT-AlN film. It was also confirmed by TEM (not shown) that the growth rate of AlN at the low temperature remains same as that at high temperature with Al/N flux ratio ~ 1 .

3. Application of MBE grown LT-AlN in HEMT

With a goal to demonstrate the application of MBE grown LT-AlN in HEMTs a series of AlN barrier GaN HEMT structures were grown by MBE with an additional LT-AlN (< 4 nm) cap layer. The HEMT structures grown underneath the LT-AlN cap consisted of GaN/HT-AlN/GaN/HT-AlN ($\sim 2/3.5/250/1$ nm) layers with ± 0.5 nm variation in the HT-AlN barrier within the series of samples. $1\text{ cm} \times 1\text{ cm}$ pieces of MOCVD grown Si GaN on sapphire were chosen as the substrate. A growth temperature of ~ 665 °C was used for all the

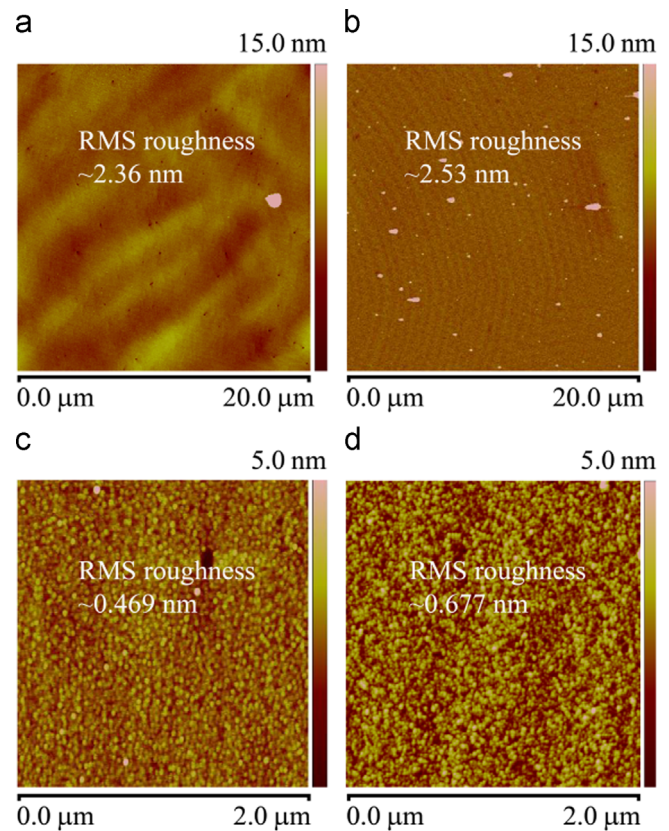


Fig. 5. AFM scan over an area of $4\ \mu\text{m}^2$ and $400\ \mu\text{m}^2$ for 15 nm AlN (a, c, respectively) and 200 nm AlN (b, d, respectively) grown at room temperature on GaN templates.

layers of the HEMT structures and GI was applied before growing the LT-AlN cap. The HT-AlN barrier and the buffer GaN layer were grown under slightly metal rich condition and N-rich condition was used for the HT-AlN nucleation layer. Indium dot contacts were formed on the as-grown HEMT structures for the Hall-effect measurement. Decently high 2DEG densities exceeding $2 \times 10^{13}\text{ cm}^{-2}$ with mobility $\sim 1000\text{ cm}^2/\text{Vs}$ and sheet resistance below $250\ \Omega/\square$ were measured at room temperature for all the samples. The Hall-effect data measured at room temperature and 77 K are illustrated in Figs. 7a and 6b. These data indicate that the LT-AlN cap layer does not have adverse effect on the carrier transport properties of the 2DEG channel formed at the HT-AlN/GaN interface. Therefore, the 2DEG channels can be employed to fabricate high performance AlN/GaN HEMTs. HEMTs with annealed Ti/Al/Ni/Au contacts were fabricated using the heterostructures containing the LT-AlN cap. We report a maximum current density of $\sim 1.6\text{ A/mm}$ at 0 V gate bias and peak extrinsic transconductance of $\sim 420\text{ mS/mm}$ at 6 V drain bias for a 55 nm long, 25 μm wide device. Low DC-RF dispersion was observed for the as-fabricated device in terms of low gate lag ($\sim 1.8\%$) and drain lag ($\sim 1.4\%$) from pulsed I - V measurement (Fig. 8a) near 1 MHz. The increase in dynamic on resistance is only $\sim 5\%$. Note that the relatively lower value of the current density at DC condition compared to the pulsed condition indicates possible self-heating of the substrate. This may be due to the low thermal conductivity of the Si GaN on sapphire substrate. However, the high drain current density approaching 2 A/mm and the low gate and drain lag ($< 2\%$) are encouraging results for further study of MBE grown LT-AlN for performance boost of III-nitride HEMTs. The transfer curves with dual sweep are plotted for drain current, gate current and extrinsic transconductance (g_m) in Fig. 8b for drain bias of 6 V. The peak g_m was measured to be $\sim 424\text{ mS/mm}$ at V_{DS} of 6 V. The reason

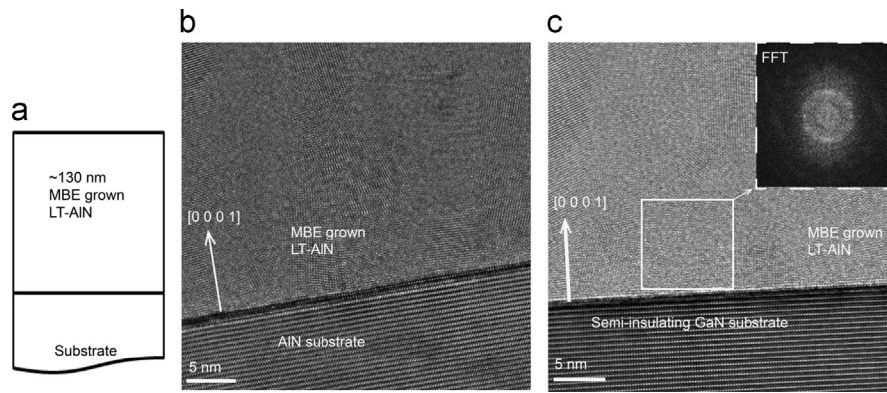


Fig. 6. Schematic of the grown structure is shown in (a). Cross section transmission electron micrographs show presence of partially amorphous regions in 130 nm LT-AlN grown on (b) AlN substrate and (c) semi-insulating GaN substrate. The inset in (c) shows FFT of the area selected by the square.

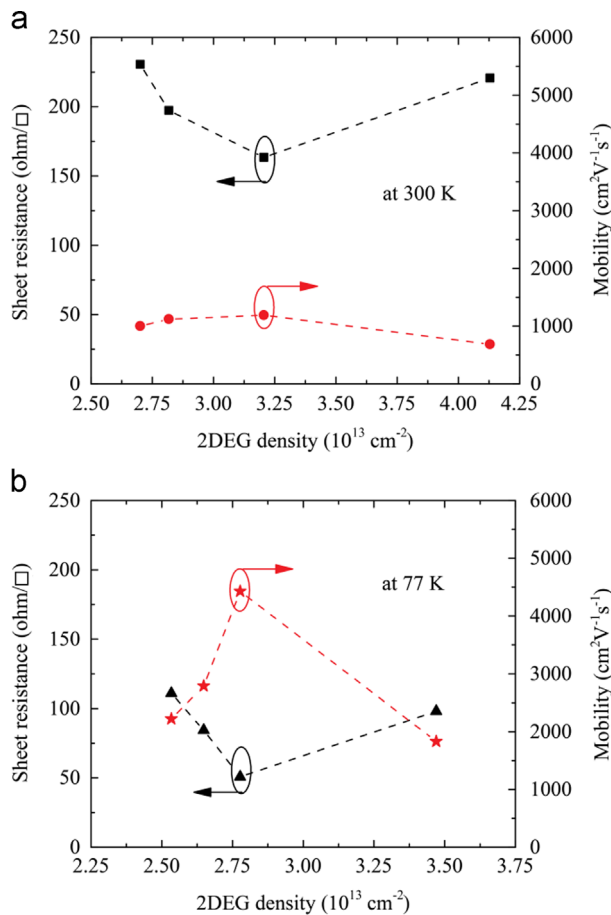


Fig. 7. Sheet resistance and mobility as a function of 2DEG density measured for the as-grown LT-AlN passivated HEMT structures at (a) room temperature (300 K) and (b) 77 K.

and mechanism of the high gate leakage will be identified in further studies where the DC performance of AlN/GaN HEMTs with LT-AlN passivation cap will be compared with control samples having no LT-AlN cap.

4. Conclusion

Low temperature growth of AlN was studied using PAMBE. Up to ~200 nm of thick crack-free LT-AlN films were grown on GaN substrate. The presence of partially amorphous regions in 130 nm

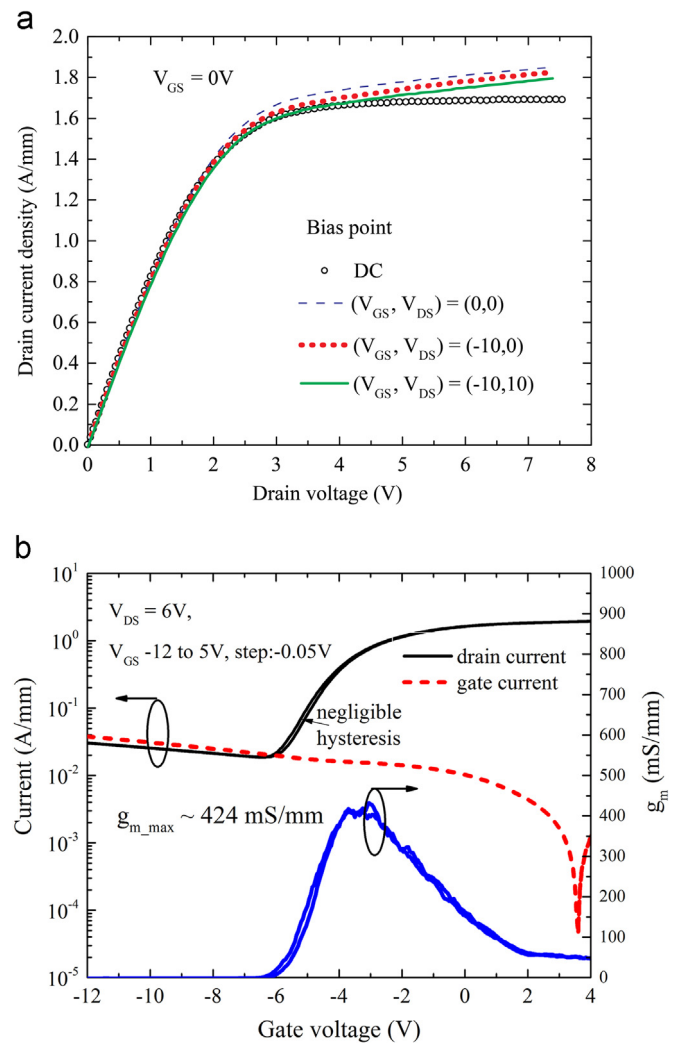


Fig. 8. (a) Pulsed I - V measured for an AlN/GaN HEMT for which MBE grown LT-AlN was applied as in-situ surface passivation. $0.3 \mu\text{s}$ wide pulses were used with a duty cycle of 99.94%. The gate is 55 nm long and $25 \mu\text{m}$ wide, (b) Transfer curves with dual sweep shown for drain current, gate current and extrinsic transconductance at a drain bias of 6 V.

thick LT-AlN film was confirmed by TEM. MBE grown LT-AlN was applied for in-situ surface passivation of AlN barrier GaN HEMT structures. Upon fabricating 55 nm long, $25 \mu\text{m}$ wide devices, low DC-RF dispersion was observed in terms of gate lag and drain lag

below 2% from pulsed I - V measurements. The HEMT showed a maximum drain current density of ~ 1.6 A/mm at 0 V gate bias and peak extrinsic transconductance of ~ 420 mS/mm at 6 V drain bias. To the best of our knowledge this is the first report of application of MBE grown LT-AlN in III-nitride HEMTs for in-situ surface passivation.

Acknowledgements

The authors would like to acknowledge the financial support from an ONR MURI grant monitored by Dr. Paul Maki.

References

- [1] S. Huang, et al., IEEE Electron Device Lett. 33 (2012) 516–518. <http://dx.doi.org/10.1109/LED.2012.2185921>.
- [2] A.D. Koehler, et al., IEEE Electron Device Lett. 34 (9) (2013) 1115–1117. <http://dx.doi.org/10.1109/LED.2013.2274429>.
- [3] J. Hwang, et al., Solid State Electron. 48 (2) (2004) 363–366. [http://dx.doi.org/10.1016/S0038-1101\(03\)00324-1](http://dx.doi.org/10.1016/S0038-1101(03)00324-1).
- [4] S.L. Selvaraj, et al., Appl. Phys. Lett. 90 (2007) 173506. <http://dx.doi.org/10.1063/1.2730751>.
- [5] J. Derluyn, et al., J. Appl. Phys. 98 (2005) 054501. <http://dx.doi.org/10.1063/1.2008388>.
- [6] D.H. Kim, et al., Electron. Lett. 43 (129) (2007), <http://dx.doi.org/10.1049/el:20073494>.
- [7] R. Wang, et al., IEEE IEDM Dig. (2013).
- [8] AlN—Aluminium Nitride. Ioffe Database.
- [9] Y. Cao, et al., Appl. Phys. Lett. 90 (2007) 182112. <http://dx.doi.org/10.1063/1.2736207>.
- [10] S. Figge, et al., Appl. Phys. Lett. 94 (2009) 101915. <http://dx.doi.org/10.1063/1.3089568>.
- [11] J.M. Khoshman et al., J. Non-Cryst. Solids, 351, 40–42, 3334–3340 (<http://dx.doi.org/10.1016/j.jnoncrysol.2005.08.009>).